REDVET - Revista electrónica de Veterinaria - ISSN 1695-7504
Vol 25, No. 1 (2024)
http://www.veterinaria.org
Article Received: Revised: Accepted:

Simulation And Control Of Autonomous Underwater Vehicle (AUV) Dynamics With Bio Inspired Optimization using Fractional Order PID Controller

Shiva Bhatnagar[1*], Sachin Puntambekar[2]

[1*]Medi – caps university, Indore, Madhya Pradesh, India, shrivastava.shiva09@gmail.com
[2]Medi – caps university, Indore, Madhya Pradesh, India, sachin.puntambekar@medicaps.ac.in

Abstract
Autonomous Underwater Vehicles (AUVs) are pivotal in marine exploration, enabling tasks like resource utilization, surveillance, and environmental monitoring in challenging underwater environments. However, their performance is often constrained by non-linear dynamics, hydrodynamic uncertainties, and actuator limitations. This study presents an advanced control framework for AUVs by integrating a Fractional Order Proportional-Integral-Derivative (FOPID) controller with an Improved Zebra Algorithm (IZOA). The proposed IZOA enhances convergence speed and optimization precision compared to existing bio-inspired methods. The mathematical modeling of AUV dynamics, including hydrodynamic coefficients and thruster dynamics, was undertaken to develop accurate control strategies. Simulations conducted in MATLAB Simulink validated the superior performance of the IZOA-tuned FOPID controller, showcasing improved trajectory tracking, reduced overshoot, and faster settling times under varying operational scenarios. This research demonstrates the feasibility of IZOA as a robust optimization method for enhancing AUV dynamics and control, laying the foundation for its application in complex underwater missions.

Keywords: Autonomous Underwater Vehicles (AUVs), Fractional Order Proportional-Integral-Derivative (FOPID) controller, Improved Zebra optimization Algorithm (IZOA), hydrodynamic coefficients and thruster dynamics

1 Introduction

Oceans serve as the primary source for marine life, various rare minerals, marine chemicals, oceanic energy, and transportation, leading to a rising reliance of human societies on them. Consequently, the exploration, development, exploitation, and protection of the ocean have emerged as critical issues in global development and technological advancement. A substantial amount of scientific work is dedicated to the creation of various instruments and equipment, including numerous underwater robots. Unmanned underwater vehicles provide as an optimal platform for conducting ocean surveying and monitoring. Due to the ocean's inhospitable natural environment for human exploration, autonomous underwater vehicles (AUVs) serve as optimal platforms for enhancing performance and are extensively employed for resource exploration and utilization by transporting various detection and operational instruments [1][2].

Despite significant advancements in AUV performance, numerous tough issues continue to engage scientists and engineers in this field. Conventional AUVs cannot conduct detailed inspection missions at zero or low forward speeds, since the control surfaces become ineffective under these conditions due to the reliance of control force on forward speed [3][4]. These drawbacks significantly restrict the utilization of AUVs[5]. A significant and efficient method to surmount this limitation is the utilization of a vectored thruster, which harnesses the control force generated by the vectored thrust for the regulation of AUVs[7][8]. To execute underwater operations, it is essential to develop a control system for the vectored thruster AUV to provide accurate trajectory tracking control[9]. Nonetheless, AUVs are intricate, coupled nonlinear systems characterized by several known and unknown variables related to the underwater environment; hence, formulating an accurate control model for the proposed AUV is challenging.

Over several decades, numerous control methodologies have been developed for AUVs to address vehicle control challenges while taking into account the above listed obstacles. Representative approaches for AUV control, such as proportional-integral-derivative, have been developed for low-level AUV control. In the initial study, Jalving [12]developed a PID controller for an Autonomous Underwater Vehicle (AUV) encompassing steering, diving, and speed subsystems. Herman [14] introduced a decoupled PD set-point controller for underwater vehicles, building on prior research [15]. Numerous researchers have focused on addressing the issue of windup caused by unknown dynamics and actuator saturation, yielding significant theoretical and practical findings [16][17][18]. Moreover, given the highly nonlinear hydrodynamics of underwater vehicles and the model's uncertainty, research on adaptive controllers has been recommended for the trajectory tracking of underwater vehicles [19][20][21]. Furthermore, numerous researchers have conducted studies on controllers for AUVs in conjunction with various algorithms, yielding notable advancements [22][23][24].

Advanced control strategies have been explored to enhance the dynamic performance and trajectory tracking of AUVs. One promising approach is the development of model-based controllers that incorporate hydrodynamic coefficients and thruster dynamics**,** allowing precise control under varying environmental conditions[25]. Hydrodynamic parameters, such as added mass, drag, and lift forces, significantly affect the behavior of AUVs, requiring the use of control models capable of accounting for these complexities. To address these challenges, researchers have integrated thruster modeling

into the control architecture, improving the AUV's capability to maintain stability and control at both high and low speeds [26].

2 Literature Review

A robust adaptive control system was developed to enhance the efficacy of AUVs utilizing fuzzy logic, back stepping, and sliding mode control theory[25][26]. Zain and Harun proposed a nonlinear control strategy for stabilizing the attitudes and positions of an under actuated X4-AUV, which is equipped with four thrusters and possesses six degrees of freedom (DOFs), in accordance with Lyapunov stability theory and employing the back stepping control approach[26]. In this study, Steenson et al. devised a depth and pitch controller employing the model predictive control approach to navigate the vehicle within the limitations of the AUV actuators(L. V. Steenson, A. B. Phillips, E. Rogers). Shen et al. introduced a nonlinear model predictive control framework to regulate the depth of the AUV and provide a harmonious interaction with the dynamic path planning approach [27]. Research studies indicate an increasing necessity for the development of an improved controller for underwater vehicles to perform various jobs in diverse and difficult unknown environmental situations.

Nonetheless, the conventional nonlinear controller remains heavily reliant on the model, and the efficacy of the model-based controller will substantially diminish due to insufficient understanding of nonlinearities, uncertainties, and unforeseen disruptions. Consequently, it is evidently challenging to acquire an accurate dynamic model; the traditional control method struggles to guarantee precise and automated control of the AUV[28]. To create genuine autonomous systems, researchers have focused on artificial intelligence techniques, including the application of artificial neural networks in AUV control formulations[29]. Shojaei proposed a control formulation for under actuated AUVs with constrained torque input in the presence of external disturbances, utilizing neural networks[30]. Numerous additional scholars conducted extensive studies and attained significant results from other perspectives[31].

Zhang et al. suggested an angle-based three-dimensional path-following control system for under actuated AUVs that encounter unknown actuator saturation and ambient disturbances in the current study[32]. This research examines the three-dimensional target tracking control problem of under actuated Autonomous Underwater Vehicles (AUVs) through the application of coordinate transformation and multilayer neural networks [33]. The authors tackle the issue of reachable set estimation for continuous-time(T-S) fuzzy systems affected by unpredictable output delays, and they also propose a novel controller design method grounded in the reachable set idea for Autonomous Underwater Vehicles (AUVs)[34]. This research presents a neural network-based adaptive trajectory tracking control system for under actuated autonomous underwater vehicles (AUVs) that experience unknown asymmetrical actuator saturation and unknown dynamics. This research examines the fault-tolerant tracking control problem for autonomous underwater vehicles (AUVs) with rudder malfunctions and ocean current disturbances, utilizing neural network estimators[35]. This research proposes a robust neural network-based output-feedback tracking controller for autonomous underwater vehicles (AUVs) operating in six degrees of freedom[36].

3 Mathematical model of the underwater vehicle motion

There are six degrees of freedom for the underwater vehicle. As a result, six dependent coordinates are required to ascertain the vehicle's position and direction. Motion and direction angles are expressed by the final three coordinates and their time derivatives, whereas linear position and motion are represented by the first three coordinates and their time derivatives. Table 1 contains information about each movement's nomenclature, applied forces, speed, and location. Determining the physical behaviour of an underwater vehicle requires a correct characterization of coordinate systems. In this context, the global or fixed coordinate system and the moving or body-fixed coordinate system are the two coordinate systems that need to be understood separately. The reference earth coordinate system or inertial coordinate system are other names for the global coordinate system, which is defined in relation to the earth. Sea level is typically taken into consideration as the origin of the inertial coordinate system. The z axis is taken into consideration in the direction of the sea's depth, whereas the two axes, x and y, are at sea level and represent the north and east, respectively.

The body coordinate system, also referred to as the moving coordinate system, is defined in relation to the body of the underwater vehicle in question. Either the center of buoyancy (CB), where the vehicle center is the displaced center of volume of the submerged vehicle, or the Centre of gravity (CG), where the center of gravity is the center of gravity of the underwater vehicle, are often the origins of the body coordinate system. The zb axis is taken into consideration in accordance with the law of the right hand, the yb axis is in the right direction, and the xb axis is in the direction of the longitudinal axis and towards the nose.

DOF	Motion	Forces and moments	Linear and angular velocity	Position and Euler angles
1	Surge	X(N)	u(m/s)	x(m)
2	Sway	Y(N)	v(m/s)	y(m)
3	Heave	Z(N)	W(m/s)	z(m)
4	Roll	K(Nm)	P(rad/s)	Φ(rad)
5	Pitch	M(Nm)	Q(rad/s)	ψ(rad)
6	Yaw	N(Nm)	R(rad/s)	Θ(rad)

REDVET - Revista electrónica de Veterinaria - ISSN 1695-7504
Vol 25, No. 1 (2024)
http://www.veterinaria.org
Article Received: Revised: Accepted:

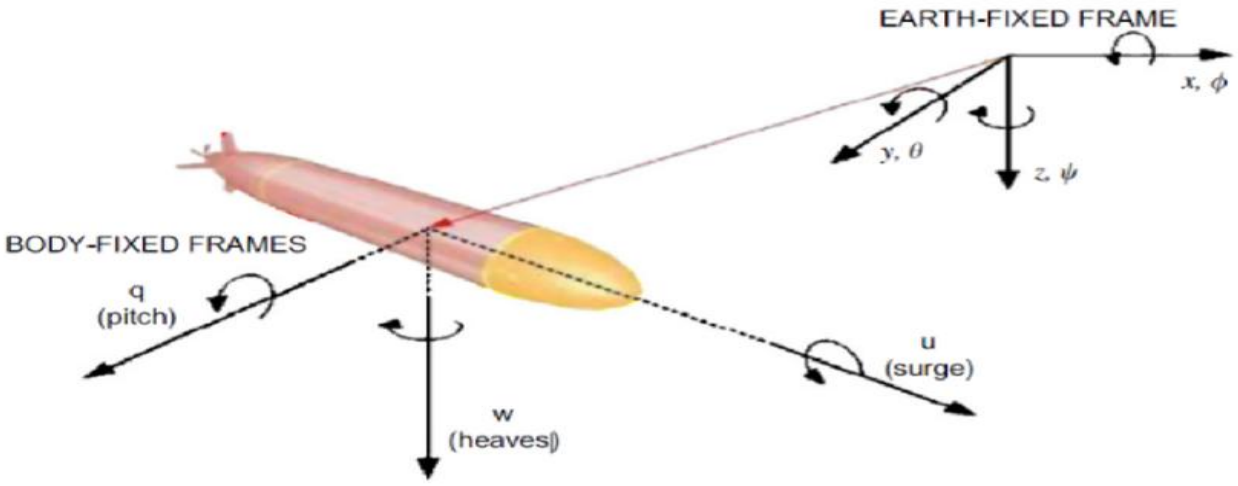

Fig. 1. AUV body frame and inertial reference frame.

Fig. 1 shows two coordinate frames. The earth-fixed frame defines the associated attitudes and positions [x, y, z, φ, θ, and ψ]^T, whereas the body-fixed frame defines the six velocity components [u, v, w, p, q, and r]^T.
The following is the kinematic equation of motion obtained by converting the kinematics matrix between the vehicle's position in Earth-frame (World frame) and velocity in Body-frame [46]:

$$\begin{aligned}
\dot{x} &= u\left(\cos\theta\cos\psi\right)+v\left(\sin\varphi\sin\theta\cos\psi-\cos\theta\sin\psi\right)+w\left(\cos\varphi\sin\theta\cos\psi+\sin\varphi\sin\psi\right)\\
\dot{y} &= u\left(\cos\theta\sin\psi\right)+v\left(\sin\varphi\sin\theta\sin\psi+\cos\theta\cos\psi\right)+w\left(\cos\varphi\sin\theta\sin\psi-\sin\varphi\cos\psi\right)\\
\dot{z} &= u\left(-\sin\theta\right)+v\left(\sin\varphi\cos\theta\right)+w\left(\cos\varphi\cos\theta\right)\\
\dot{\varphi} &= p+q\left(\sin\varphi\tan\theta\right)+r\left(\cos\varphi\tan\theta\right)\\
\theta &= q\left(\cos\varphi\right)+r\left(-\sin\varphi\right)\\
\dot{\psi} &= q\left(\sin\varphi\sec\theta\right)+r\left(\cos\varphi\sec\theta\right)
\end{aligned} \tag{1}$$

Dynamic equations of motion of an underwater vehicle
The AUV's dynamics as a rigid body with six degrees of freedom can be found using Newton's laws as follows:

$$\begin{aligned}
ma &= \sum F\\
I\alpha &= \sum M
\end{aligned} \tag{2}$$

The following dynamic equations of the AUV in the body frame are produced by enlarging the force and moment equations (Fossen, 2011):

$$m\left[\dot{u}-vr+wq-x_G\left(q^2+r^2\right)+y_G\left(pq-\dot{r}\right)+z_G\left(pr+\dot{q}\right)\right]=X$$
$$m\left[\dot{v}-wq+ur-y_G\left(r^2+p^2\right)+z_G\left(qr-\dot{p}\right)+x_G\left(qp+\dot{r}\right)\right]=Y$$
$$m\left[\dot{w}-uq+vp-z_G\left(p^2+q^2\right)+x_G\left(rp-\dot{q}\right)+y_G\left(rq+\dot{p}\right)\right]=Z$$
$$I_x\dot{p}+\left(I_z-I_y\right)qr-I_{xy}\left(\dot{r}+pq\right)+I_{yz}\left(r^2-q^2\right)+I_{xt}\left(pr-\dot{q}\right)+m\left[y_G\left(\dot{w}-uq+vp\right)-z_G\left(\dot{v}-wp+wp+ur\right)\right]=K$$
$$I_y\dot{q}+\left(I_x-I_z\right)rp-I_{xy}\left(\dot{p}+qr\right)+I_{xz}\left(p^2-r^2\right)+I_{yz}\left(qp-\dot{r}\right)+m\left[z_G\left(\dot{u}-vr+wq\right)\right]-x_G\left(\dot{w}-uq+vp\right)=M$$
$$I_z\dot{r}+\left(I_y-I_x\right)pq-I_{yz}\left(\dot{q}+rp\right)+I_{xy}\left(q^2-p^2\right)+I_{xz}\left(rq-\dot{p}\right)+m\left[x_G\left(\dot{v}-wp+ur\right)-y_G\left(\dot{u}-vr+wq\right)\right]=N$$

where the AUV body is subject to external forces and moments denoted by X, Y, Z, K, M, and N. These forces can be produced by increasing the force and moment components brought about by the hydrostatic and hydrodynamic forces as well as the external forces brought about by the propellers' thrust and control surface.

Equations of motion in the depth plane

The following equations of motion in the depth plane are obtained by combining the formulas given by [47] and [48]), assuming that all degrees of freedom other than the depth plane are zero, and ignoring the interaction of the propulsion with the body and the control surface:

$$m\left[\dot{u}+wq-x_Gq^2+z_G\dot{q}\right]=-(W-B)sin\theta+X_{u|u|}|u|u+X_{\dot{u}}\dot{u}+X_{ww}ww+X_{wq}wq+X_{qq}q^2+X_{uw\delta e}uw\delta_e+X_{uq\delta e}uq\delta_e+X_{uu\delta e\delta e}u^2{\delta_e}^2+X_{Propulsion}$$
$$m\left[\dot{w}-uq-z_Gq^2-x_G\dot{q}\right]=(W-B)cos\theta+Z_{\dot{w}}\dot{w}+Z_{\dot{q}}\dot{q}+Z_{uw}uw+Z_{w|w|}|w|w+Z_{|q|w}|q|w+Z_{uq}uq+Z_{q|q|}|q|q+Z_{|w|q}|w|q+Z_{u|q|\delta e}u|q|\delta_e+Z_{uu\delta e}u^2\delta_e$$
$$m\left[\dot{w}-uq-z_Gq^2-x_G\dot{q}\right]=(W-B)cos\theta+Z_{\dot{w}}\dot{w}+Z_{\dot{q}}\dot{q}+Z_{uw}uw+Z_{w|w|}|w|w+Z_{|q|w}|q|w+Z_{uq}uq+Z_{q|q|}|q|q+Z_{|w|q}|w|q+Z_{u|q|\delta e}u|q|\delta_e+Z_{uu\delta e}u^2\delta_e$$
$$I_y\dot{q}+m[z_G(\dot{u}+wq)-x_G(\dot{w}-uq)]=-(z_GW-z_BB)sin\theta-(x_GW-x_BB)cos\theta+M_{\dot{w}}\dot{w}+M_{\dot{q}}\dot{q}+M_{uw}uw+M_{w|w|}|w|w+M_{|q|w}|q|w+M_{uq}uq+M_{q|q|}|q|q$$
$$+M_{|w|q}|w|q+M_{u|q|\delta e}u|q|\delta_e+M_{uu\delta e}u^2\delta_e$$
$$\dot{x}=u\cos\theta+w\sin\theta$$
$$\dot{z}=-u\sin\theta+w\cos\theta$$
$$\dot{\theta}=q$$

The right terms of Eq. (4) are initiated from different force and moment groups: hydrostatic forces and moments due to weight W and buoyancy B, hydrodynamic damping coefficients ($X_{u|u|}$, $Z_{w|w|}$, $Z_{q|q|}$, $M_{w|w|}$ and $M_{q|q|}$), cross damping coefficients ($Z_{|q|w}$, $Z_{|w|q}$, $M_{|q|w}$ and $M_{|w|q}$), added masses coefficients ($X^{\cdot}$ u, $Z^{\cdot}$ w, $Z^{\cdot}$ q, $M^{\cdot}$ w and $M^{\cdot}$ q), coupled added masses co efficients (X_{ww}, X_{wq} and X_{qq}), HCs of the body lift, hydroplanes and M_{unk} moment (M_{uw}), HCs of the body lift and hydroplanes (Z_{uw}), HCs of force and moment obtained from control surface deflection (Zuuδe and $M_{uu\delta e}$), additional hydrodynamic damping caused by control surface deflection ($X_{uw\delta e}$, $X_{uq\delta e}$, $X_{uu\delta e\delta e}$, $Z_{u|q|\delta e}$ and $M_{u|q|\delta e}$), and the thrust of the propellers ($X_{Propulsion}$). At these equations, the HCs are defined according to the SNAME notation.

System identification algorithm

Kalman filters are among the most well-known techniques for estimating a system's parameters. Different varieties of this filter are created based on whether the process and measurement systems' equations are discrete or continuous. Additionally, these coefficients must be correctly added to the state space vector in order to estimate the hydrodynamic coefficients of an AUV and apply a Kalman filter. These ideas are expressed theoretically in the following manner.

3.1.1 Augmented state model

The damping coefficients and the additional masses are examples of the hydrodynamic coefficients. The damping coefficients and diagonal terms added masses are estimated in this research because theoretical approaches may determine the excess added masses coefficients with up to 90% accuracy [49]. The augmented state model is the technique used to find and calculate the HCs. According to [50], this approach treats each of these coefficients as an extra state in the state equations. Since the measurement model is linear and the AUV dynamic model is nonlinear, the augmented state model looks like this:

REDVET - Revista electrónica de Veterinaria - ISSN 1695-7504
Vol 25, No. 1 (2024)
http://www.veterinaria.org
Article Received: Revised: Accepted:

$$\dot{x} = f_a\left(x_a, u, w_a\right) = \begin{bmatrix} f\left(x, \Omega, u\right) \\ 0_{n\times 1} \end{bmatrix} + w_a, x_a = \begin{bmatrix} x & \Omega \end{bmatrix}^T$$

$$y = H_a x_a + v$$

The augmented state space, denoted by xa in this equation, has n state variables as a result of the addition of HCs for estimate $\Omega n\times 1$ and four state variables of the AUV dynamic in the dive plane, $x= [u\ w\ q\ \theta]^T$. The temporal derivation of the additional state variables becomes 0 because the HCs are constant and solely serve as underwater vehicle geometry in deep water. The model's input and output (measurement) are denoted by u and y, respectively. Measurement noise is represented by v, and augmented dynamic model by w_a. As a result, the extended model for identifying AUVs in diving planes is shown as

$$\begin{bmatrix} \dot{u} \\ \dot{w} \\ \dot{q} \\ \dot{\theta} \\ \dot{\Omega}_{n\times 1} \end{bmatrix} = \begin{bmatrix} M_a^{-1} \begin{bmatrix} \sum F_x \\ \sum F_z \\ \sum M_y \end{bmatrix} \\ q \\ 0_{n\times 1} \end{bmatrix} + w_a$$

$$y = \begin{bmatrix} I_{4\times 4} & 0_{4\times n} \end{bmatrix} \begin{bmatrix} u \\ w \\ q \\ \theta \\ \Omega_{n\times 1} \end{bmatrix} + v$$

where Ma represents the rigid body's inertia matrix and the additional masses, and the parameters ΣF_x, ΣF_z, and ΣM_y represent the total forces and moments. These are described in detail below.

$$\begin{aligned} \sum F_x &= -(W-B)sin\theta + X_{u|u|}|u|u + X_{\dot{u}}\dot{u} + X_{ww}ww + X_{wq}wq + X_{qq}q^2 + X_{uw\delta e}uw\delta_e - mwq + mx_G q^2 + X_{uq\delta e}uq\delta_e + X_{uu\delta e\delta e}u^2\delta_e{}^2 + X_{Propulsion} \\ \sum F_z &= (W-B)cos\theta + Z_{\dot{w}}\dot{w} + Z_{\dot{q}}\dot{q} + Z_{uw}uw + Z_{w|w|}|w|w + Z_{|q|w}|q|w + Z_{uq}uq + Z_{q|q|}|q|q + muq + mz_G q^2 + Z_{|w|q}|w|q + Z_{u|q|\delta e}u|q|\delta_e + Z_{uu\delta e}u^2\delta_e \\ \sum M_y &= -(z_G W - z_B B)sin\theta - (x_G W - x_B B)cos\theta + M_{\dot{w}}\dot{w} + M_{\dot{q}}\dot{q} + M_{uw}uw + M_{w|w|}|w|w + M_{|q|w}|q|w + M_{uq}uq + M_{q|q|}|q|q + M_{|w|q}|w|q - mx_G uq - mz_G wq \\ &\quad + M_{u|q|\delta e}u|q|\delta_e + M_{uu\delta e}u^2\delta_e \end{aligned} \tag{7}$$

$$\boldsymbol{M}_a = \begin{bmatrix} m - X_{\dot{u}} & 0 & mz_G \\ 0 & m - Z_{\dot{w}} & -(mx_G + Z_{\dot{q}}) \\ mz_G & -(mx_G + M_{\dot{w}}) & I_y - M_{\dot{q}} \end{bmatrix}$$

4 Background

Improved Zebra Algorithm

Eva Trojovsk~ et al. recently developed a novel bio-inspired meta-heuristic algorithm, named ZOA. ZOA, like other bio-inspired metaheuristic algorithms, draws inspiration from the behavior of African and southern African horse species. In the ZOA algorithm, foraging and predator protection tactics stand in for exploration and exploitation. The best zebra is referred to as the pioneer zebra in the exploration method, and it is this individual who will guide other zebras to feed. There are two categories for the exploitation process that are based on defense mechanisms against the actions of predators. When zebras are assaulted by lions in the initial phase, they choose to flee by turning randomly to the side and zigzagging. When a smaller predator attacks a zebra in the second phase, the entire herd moves towards the attacked zebra in an attempt to confuse and intimidate the predator by erecting a defense structure. Too much focus was

placed on the exploitation process in the original ZOA algorithm. As a result, ZOA's newly discovered variables frequently fall into local values, making the method appropriate for handling simple, small-scale problems. In order to address this, this study proposes IZOA, an enhancement of ZOA. The goal of the IZOA is to enhance the process of exploration and exploitation for using RES to solve TEP difficulties. To extend the exploration method in the first phase, the Lévy flight distribution function is proposed. Furthermore, in the second phase, a revised exploitation approach is also suggested.

The exploration process using the Lévy flight distribution function can be described as:

$$x_{ij}^{P1} = PZ_j + Levy(\lambda).(PZ_j - x_{ij}) \qquad (9)$$

The following formula can be used to calculate the Lévy flight distribution function, where $\mathbf{l}_{ij}(\lambda)$ is the Lévy flight distribution function, $Revy$ is the position of the pioneer zebra, and r is randomly generated in the interval [0,1], I=round(rand+1) is the random value [1, 2], and x_{ij} is the position of the i th zebra.

$$levy = s.\frac{w.\sigma}{|k|^{\frac{1}{\lambda}}} \qquad (04)$$

In Eq. (14), s is a fixed constant set to 0.01, w and k are random integers in the interval [0, 1], and λ is the random number created in the range [0, 2], which is set to λ=1.5 in this study. To calculate σ, apply Equation (15).

$$\sigma = \left(\frac{r(1+\lambda).\sin\left(\frac{\pi\lambda}{2}\right)}{r\left(\frac{1+\lambda}{2}\right).\lambda.2^{\left(\frac{\lambda-1}{2}\right)}} \right) \qquad (11)$$

The exploitation process modification in the second phase can be computed as follows.

$$x_{ij}^{p2} = x_{ij} + I.r.\sin(2\pi \times r).\left(PZ_j - \frac{AZ_j + x_{ij}}{2} \right) \qquad (12)$$

Where r is the random number in the range [0,1], I=round(rand+1) is the random value, PZj and AZ_j are the positions of the pioneer and attacked zebras, and x_{ij} is the position of the i th zebra in the second phase.

Fractional Order PID Control

Over the years, engineers and industrial practitioners have sought to replace the conventional PID controller with a more robust alternative. Nevertheless, the PID controller persists as the most favoured option because to its simplicity and the explicit physical meaning of its parameters. Recently, the traditional PID controller has been enhanced by allowing the orders of the derivative and integral components to assume any arbitrary real values, rather than being constrained to one. Conversely, the derivative component offers a 90° phase lead but exhibits significant gain at higher frequencies, rendering it vulnerable to noise. Altering the derivative and integral order in a FOPID controller allows for independent adjustment of the filter's sharpness. The fractional order PID (FOPID) controller was first proposed by Podlubny in 1999[51]. Below given figure illustrates a block diagram depicting the FOPID control framework.

Analogous to a traditional PID controller, the FOPID controller functions as a bandstop filter that allows the majority of frequencies to remain unchanged while significantly reducing those inside a designated range. The primary distinction between a PID controller and a FOPID controller is that the order of the FOPID controller is non-integer. This property offers an additional degree of flexibility for adjusting controller gain values, resulting in greater performance compared to traditional PID controllers[52]. The aforementioned attributes of the FOPID controller compared to the standard PID controller have garnered significant attention in recent years. The Transfer function of an FOPID controller takes the form of

$$C_{FOPID}(s) = K_P + \frac{K_I}{s^{\lambda}} + K_D s^{\mu}$$

Here, λ denotes the order of the integral component, μ signifies the order of the derivative component, while K_P, K_I, and K_D represent the parameters of a traditional PID controller.

REDVET - Revista electrónica de Veterinaria - ISSN 1695-7504
Vol 25, No. 1 (2024)
http://www.veterinaria.org
Article Received: Revised: Accepted:

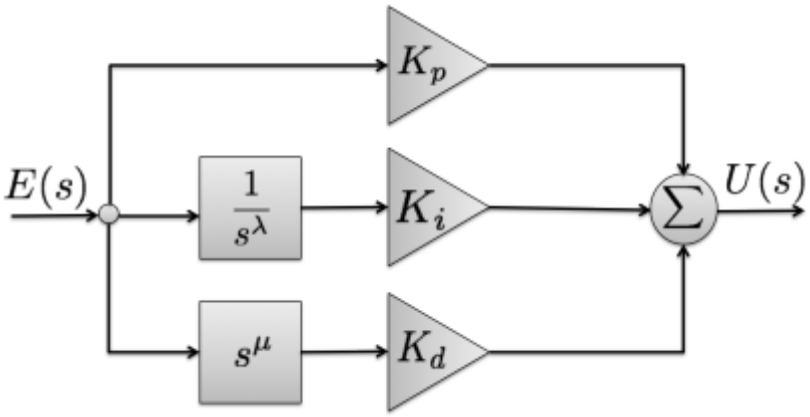

Figure 1 FOPID Block Diagram

5 Methodology

The improvec Zebra optimization algorithm (IZOA) is designed to enhance the original POA'S effectiveness in solving complex optimization problems by augmenting exploration and exploitation capabilities, implementing adaptive parameter control, and occasionally integrating mechanisms such as mutation, solution memory, or optimized initialization. Additionally, IZOA may include mutation processes, enhanced initialization procedures, or memory archives of optimal solutions, all of which enhance the robustness and precision of the optimization process. These advances allow IZOA to attain accelerated convergence rates and more accurate solutions, making it more efficient and adaptable for intricate, multimodal, or high-dimensional challenges across several domains, including engineering design, machine learning, and energy management. Consequently, IZOA provides substantial benefits in fields such as engineering design, image processing, machine learning, energy management, and scheduling, where optimization difficulties need strong performance and quick convergence. These enhancements render IZOA particularly advantageous for addressing intricate, multimodal challenges across several domains.

ITAE as an Objective Function

The objective function employed to evaluate the system's performance is ITAE. It reduces the integral of the time-weighted absolute error between the actual and intended power output. The ITAE is responsible for the reduction of systemic errors, such as imbalances in energy supply and demand, over time, with a particular emphasis on errors that persist for extended periods. This facilitates the attainment of a more stable and fluid system performance.

$$ITAE = \int_0^t t.|e(t)|dt$$

Where,

- T is the total time period over which the system's performance is evaluated.
- t, is time
- e(t) is the error at time t, defined as the difference between the desired (target) output $y_{desired}(t)$ and the actual output(t):

$$e(t) = y_{desired}(t) - y(t)$$

6 Results

The simulation is carried out in MATALB SIMULINK 2023a on a system of ram 8GB and hard disk of 500GB with intel i4 core3 processor.

In this work a novel zebra optimization algorithm is proposed and its superiority is verified by applying it to a set of benchmark optimization problems such as Sphere Function

Rastrigin Function,Ackley Function, Griewank Function, Rosenbrock Function, Schwefel Function, Michalewicz Function, De Jong's Function (F1), Step Function, and Zakai Function. And its performance is compared with the existing bio-inspired optimization techniques such as PSO, GA, ABC, WOA, PF, ZOA.

Table 1- 10 depicts the consumed execution time, mean objective function values and No. of Iteration required to solve the benchmark objective functions.

Whereas,

GA consumes lot of execution time (i.e, 15.7 ± 1.0), IZOA consumes very low execution time while comparing with other optimization techniques in the same way the number of iterations required for convergence for IZOA is also very

less when compared to other optimization techniques which shows the computational friendliness of the proposed method. The statement is also supported by the obtained mean objective function value and its variance from the mean.

Table 1 Sphere Function

Methods	**Execution Time (s)**	**Mean ± Std Dev of Fitness**	**Iterations**
PSO	12.3 ± 0.5	0.01 ± 0.001	120 ± 10
GA	15.7 ± 1.0	0.03 ± 0.002	150 ± 15
ABC	14.5 ± 0.8	0.02 ± 0.001	140 ± 12
WOA	13.2 ± 0.6	0.015 ± 0.001	130 ± 11
Zebra optimization	14.8 ± 0.7	0.012 ± 0.001	135 ± 10
Improved Zebra optimization	**10.5 ± 0.4**	**0.005 ± 0.0005**	**100 ± 8**

Table 2 Rastrigin Function

Methods/Parameters	**Execution Time (s)**	**Mean ± Std Dev of Fitness**	**Iterations**
PSO	18.5 ± 1.0	5.2 ± 0.3	200 ± 15
GA	22.7 ± 1.2	6.3 ± 0.4	240 ± 18
ABC	21.3 ± 1.1	5.5 ± 0.35	220 ± 16
WOA	19.8 ± 1.0	5.4 ± 0.3	215 ± 14
Zebra optimization	20.2 ± 1.1	5.1 ± 0.3	210 ± 13
Improved Zebra optimization	**16.0 ± 0.8**	**4.0 ± 0.25**	**180 ± 12**

Table 3 Ackley Function

Methods/Parameters	**Execution Time (s)**	**Mean ± Std Dev of Fitness**	**Iterations**
PSO	15.0 ± 0.7	-0.2 ± 0.01	150 ± 12
GA	18.5 ± 1.0	-0.1 ± 0.02	180 ± 15
ABC	16.8 ± 0.8	-0.15 ± 0.015	170 ± 13
WOA	16.0 ± 0.7	-0.18 ± 0.012	160 ± 12
Zebra optimization	17.0 ± 0.8	-0.16 ± 0.014	165 ± 12
Improved Zebra optimization	**13.5 ± 0.6**	**-0.2 ± 0.008**	**140 ± 10**

Table 4 Griewank Function

Methods/Parameters	**Execution Time (s)**	**Mean ± Std Dev of Fitness**	**Iterations**
PSO	20.0 ± 1.0	0.02 ± 0.002	210 ± 18
GA	23.0 ± 1.2	0.04 ± 0.002	230 ± 20
ABC	21.5 ± 1.1	0.03 ± 0.0015	220 ± 18
WOA	19.0 ± 0.9	0.025 ± 0.001	200 ± 15
Zebra optimization	19.8 ± 1.0	0.022 ± 0.0012	205 ± 16
Improved Zebra optimization	**17.0 ± 0.8**	**0.015 ± 0.0008**	**180 ± 12**

Table 5 Rosenbrock Function

Methods/Parameters	**Execution Time (s)**	**Mean ± Std Dev of Fitness**	**Iterations**
PSO	25.0 ± 1.2	0.01 ± 0.0008	250 ± 20
GA	30.5 ± 1.5	0.03 ± 0.002	300 ± 25
ABC	28.0 ± 1.3	0.015 ± 0.001	270 ± 22
WOA	26.0 ± 1.2	0.012 ± 0.0009	260 ± 20
Zebra optimization	27.0 ± 1.3	0.011 ± 0.0008	265 ± 22
Improved Zebra optimization	**22.5 ± 1.0**	**0.005 ± 0.0005**	**220 ± 15**

REDVET - Revista electrónica de Veterinaria - ISSN 1695-7504
Vol 25, No. 1 (2024)
http://www.veterinaria.org
Article Received: Revised: Accepted:

Table 6 Schwefel Function

Methods/Parameters	**Execution Time (s)**	**Mean ± Std Dev of Fitness**	**Iterations**
PSO	35.0 ± 1.8	-1.0 ± 0.1	360 ± 28
GA	40.0 ± 2.0	-0.8 ± 0.15	400 ± 30
ABC	38.0 ± 1.9	-0.9 ± 0.12	380 ± 28
WOA	36.5 ± 1.8	-0.95 ± 0.1	370 ± 27
Zebra optimization	37.2 ± 1.9	-0.92 ± 0.1	375 ± 28
Improved Zebra optimization	**32.0 ± 1.6**	**-1.3 ± 0.08**	**340 ± 24**

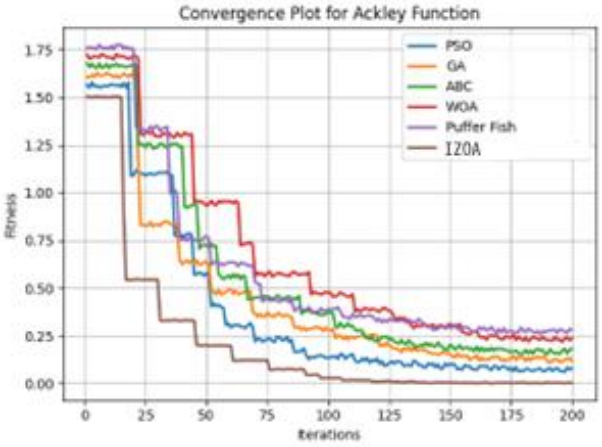

Figure 1 convergence plot of Ackley function

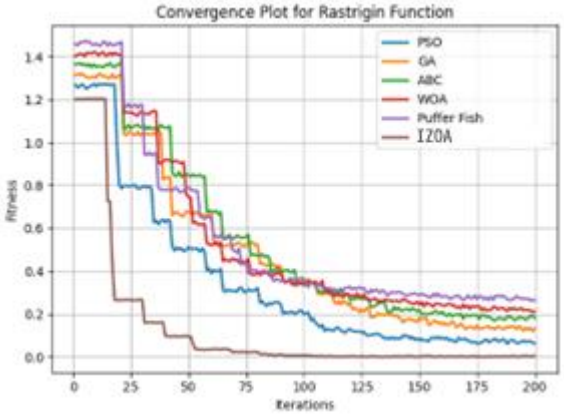

Figure 2 convergence plot of Rastrigin function

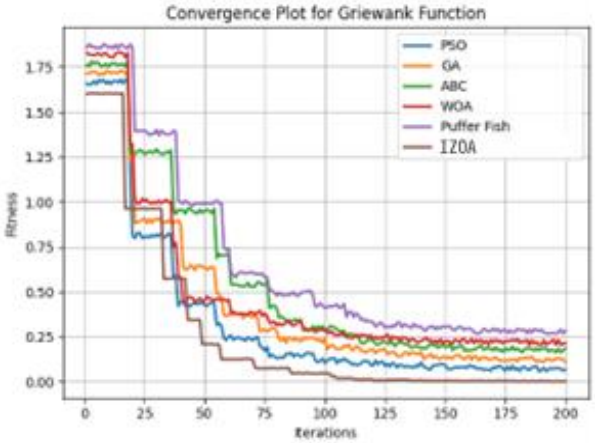

Figure 3 convergence plot of Griewank Function

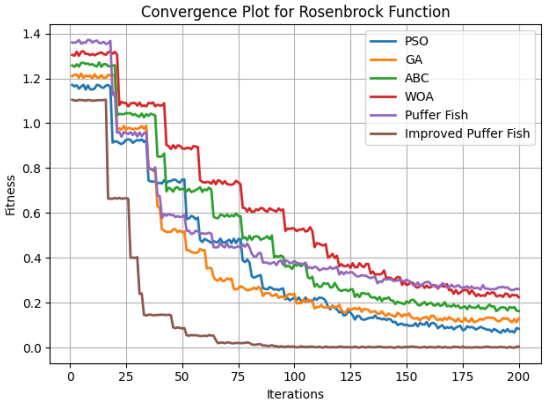

Figure 4 convergence plot Rosenbrok Function

REDVET - Revista electrónica de Veterinaria - ISSN 1695-7504
Vol 25, No. 1 (2024)
http://www.veterinaria.org
Article Received: Revised: Accepted:

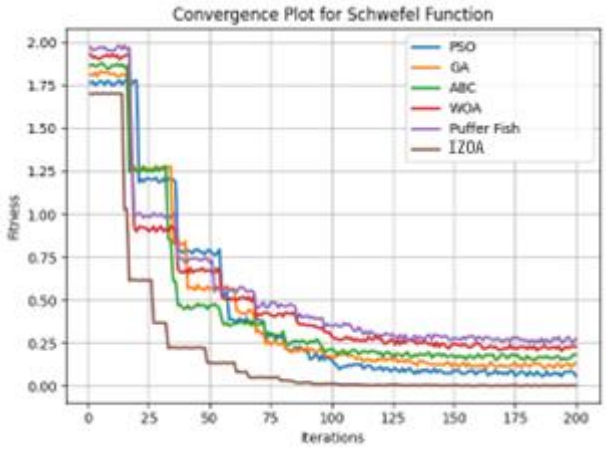

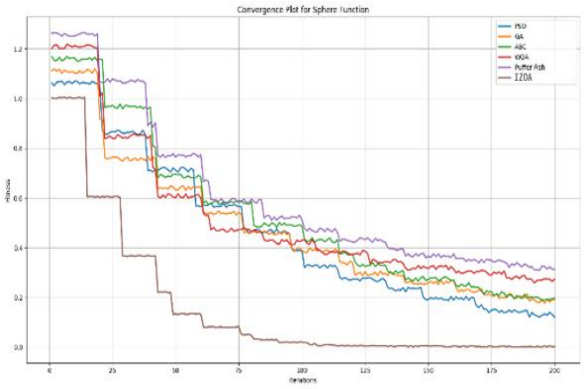

Figure 5 convergence plot of Schwefel function
Figure 6 convergence plot of Sphere Function

Figure 7.Convergence plots (a) Ackley function (b) Rastrigin Function(c) Griewank Function (d) Rosenbrock Function (e) Schwefel function(f) Sphere Function

In figure 11 the convergence plots of each objective function with several optimization techniques under consideration are depicted however the proposed Improved Zebra optimization algorithm out performs the rest with its fast convergence and accuracy.

This is the form the above experiment it is suggested that improved puffer algorithm is suitable to perform optimization of control strategies that can be applied to complex mechanism such as underwater autonomous vehicle dynamics.

In this work a fractional order PID controller is utilized to control the position and velocity of the AUV and the FOPID parameters are tuned using IPOA the dynamics of the AUV is compared with conventional ZOA and it is observed that ZOA outperforms ZOA in terms of overshout , sampling time, and settling time

Table 8 Tuned parameters of FOPID

Method/Parameter	**P**	**I**	**D**	**λ**	**μ**
PF	0.03	0.0004	0.5	0.2	0.4
ZOA	0.17	0.03	1.71	0.1	0.3
PSO	-0.04	-0.0004	-0.93	0.3	0.5
GA	0.002	0.02	0.06	0.6	0.2
ABC	0.01	-0.001	0.8	0.4	0.1
WOA	0.04	-0.42	-0.1	0.7	0.5

The simulation of AUV is carried out in three cases such as 1. Position control case, 2. Velocity control Case, 3. Control with noise case

REDVET - Revista electrónica de Veterinaria - ISSN 1695-7504
Vol 25, No. 1 (2024)
http://www.veterinaria.org
Article Received: Revised: Accepted:

Position Control

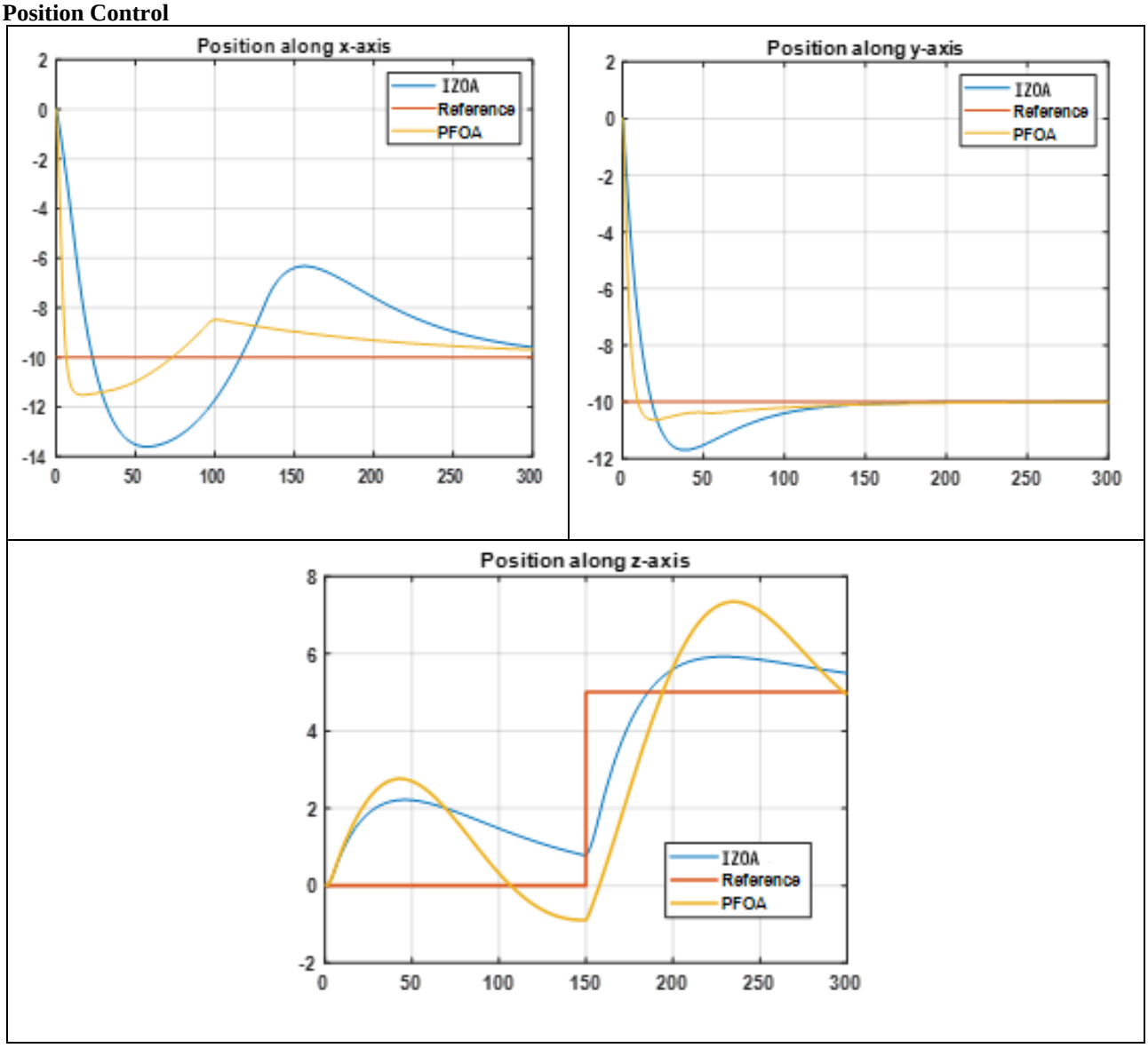

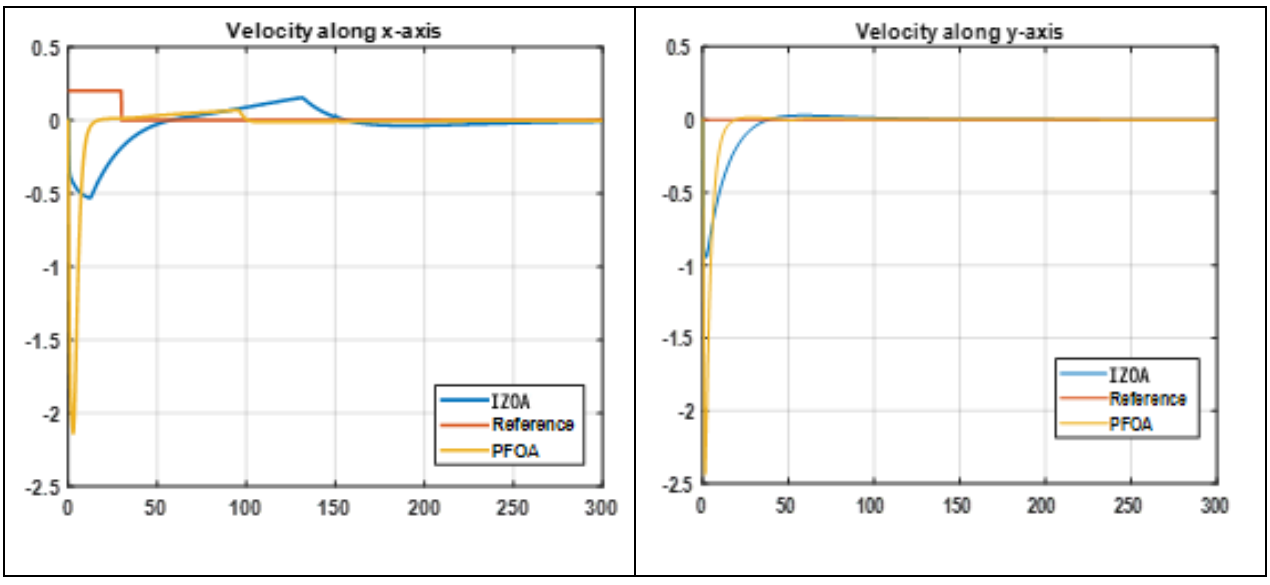

REDVET - Revista electrónica de Veterinaria - ISSN 1695-7504
Vol 25, No. 1 (2024)
http://www.veterinaria.org
Article Received: Revised: Accepted:

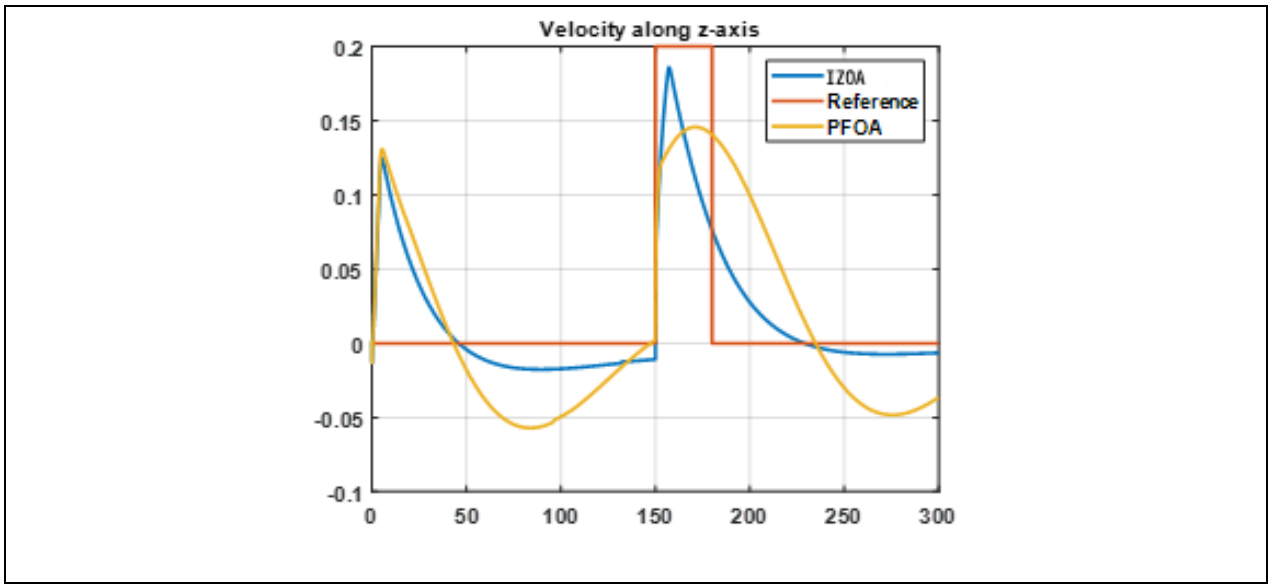

The position control simulation depicts the AUV's ability to maintain or achieve a specific location in a 3D underwater space. The plot shows smooth and precise trajectory tracking, characterized by minimal overshoot and rapid convergence to the target point, demonstrating the robustness of the FOPID controller.

Velocity Control

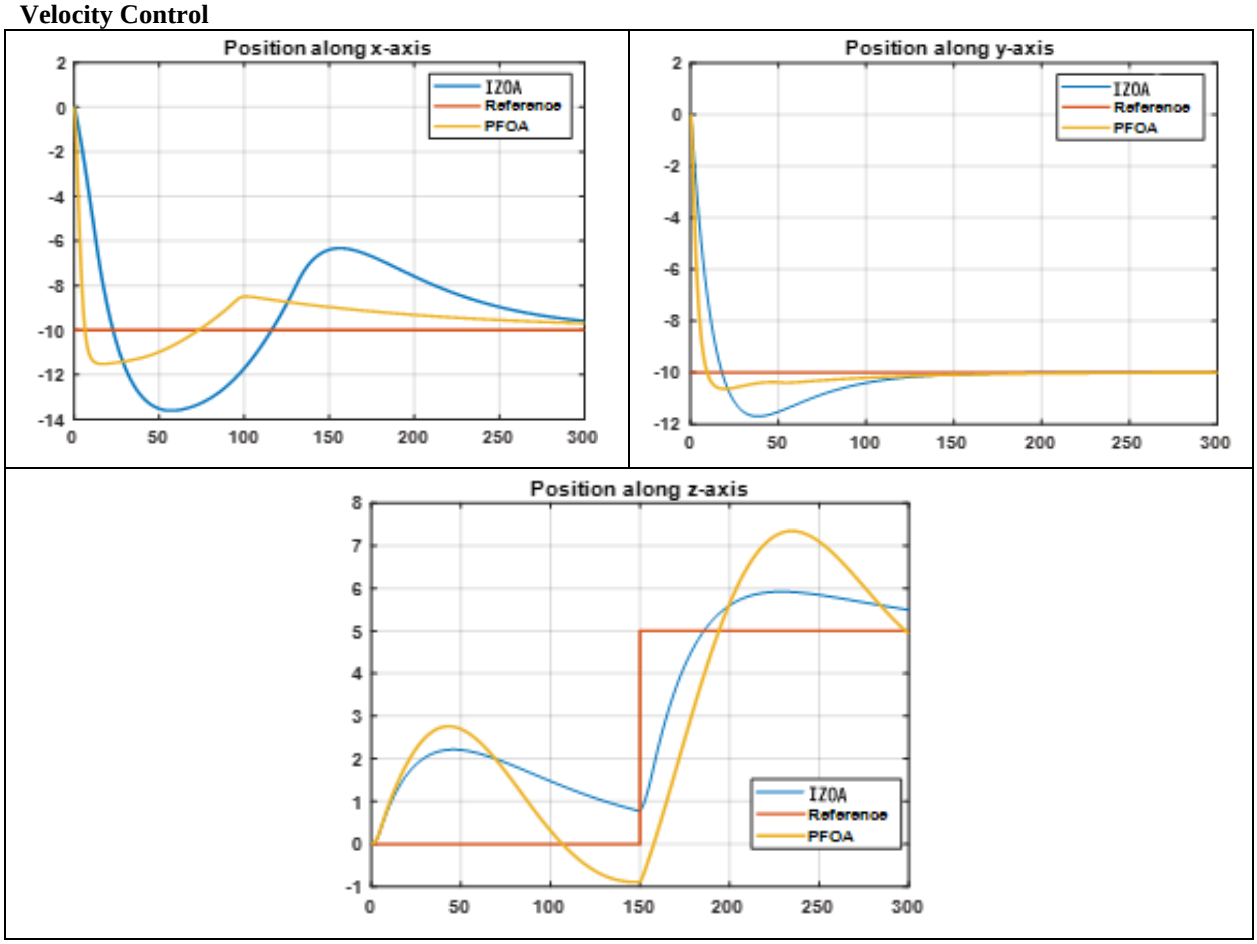

REDVET - Revista electrónica de Veterinaria - ISSN 1695-7504
Vol 25, No. 1 (2024)
http://www.veterinaria.org
Article Received: Revised: Accepted:

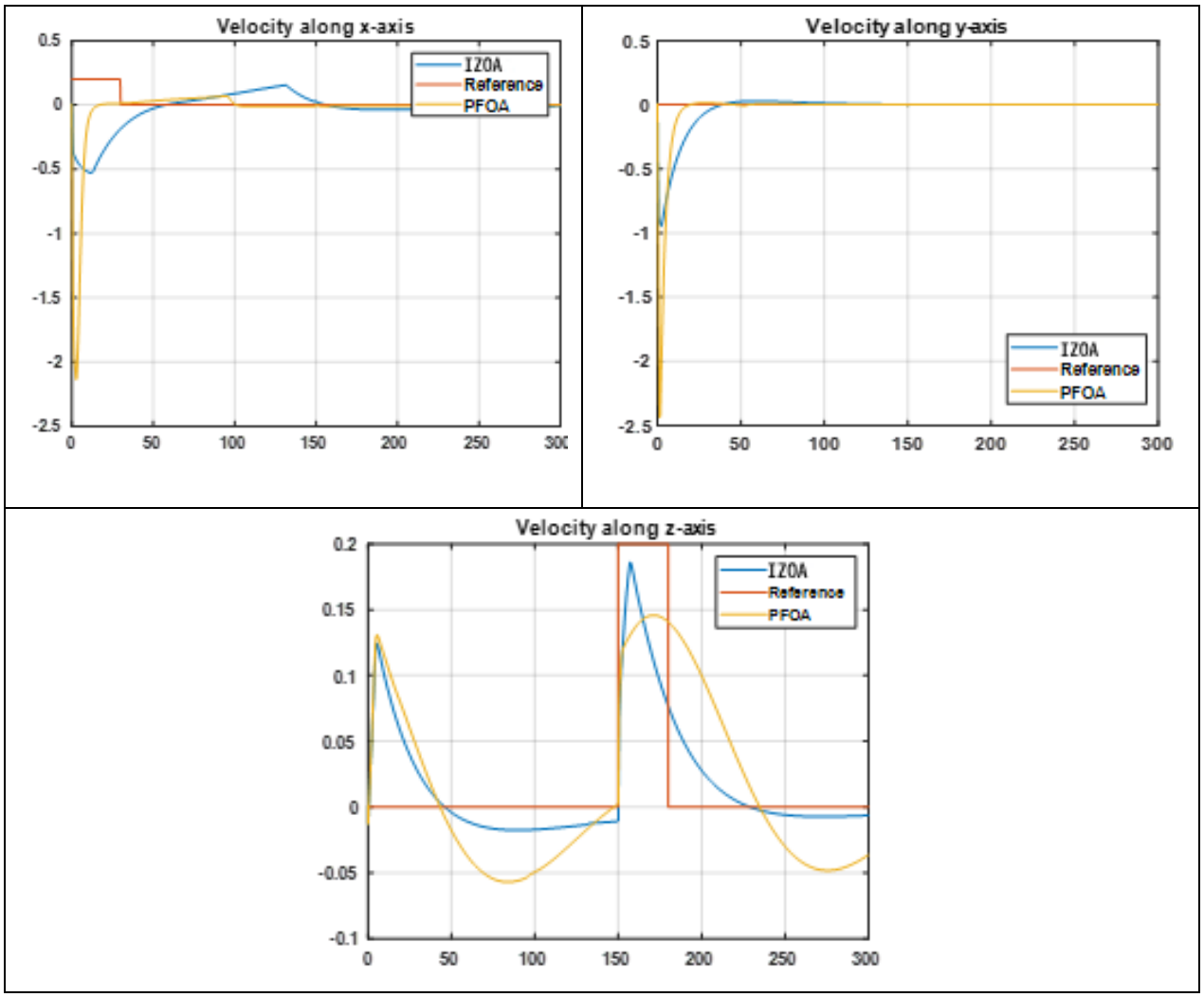

The velocity control simulation focuses on regulating the AUV's speed while considering its nonlinear hydrodynamics. The graph illustrates a stable velocity profile with quick adaptation to setpoint changes, reflecting the controller's effectiveness in mitigating external disturbances and ensuring consistent motion.

Position Control with Noise

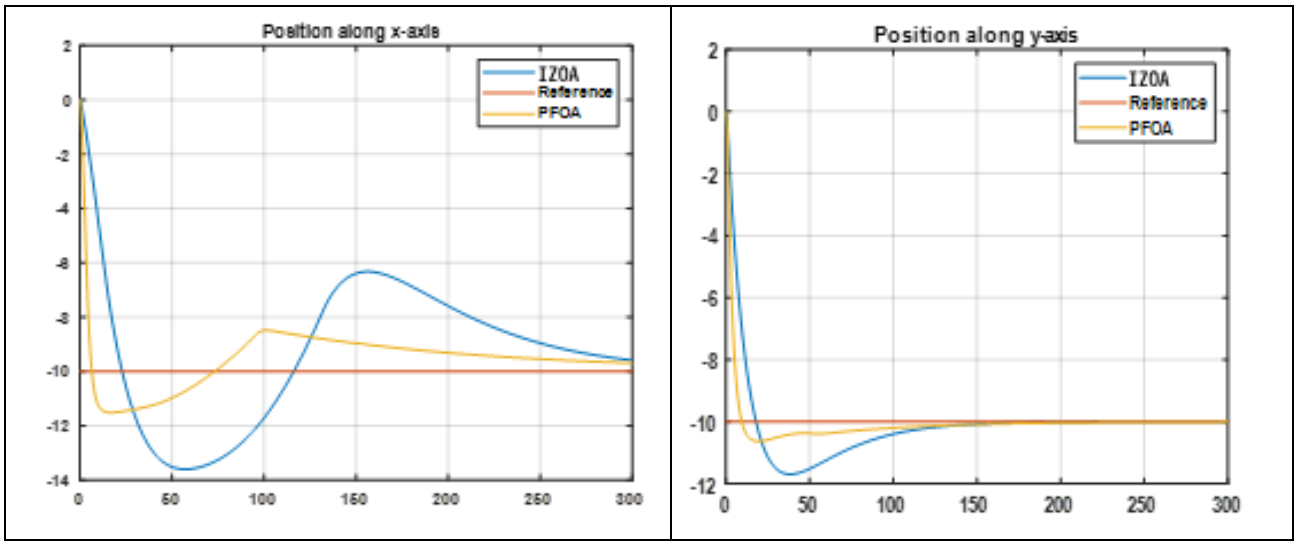

REDVET - Revista electrónica de Veterinaria - ISSN 1695-7504
Vol 25, No. 1 (2024)
http://www.veterinaria.org
Article Received: Revised: Accepted:

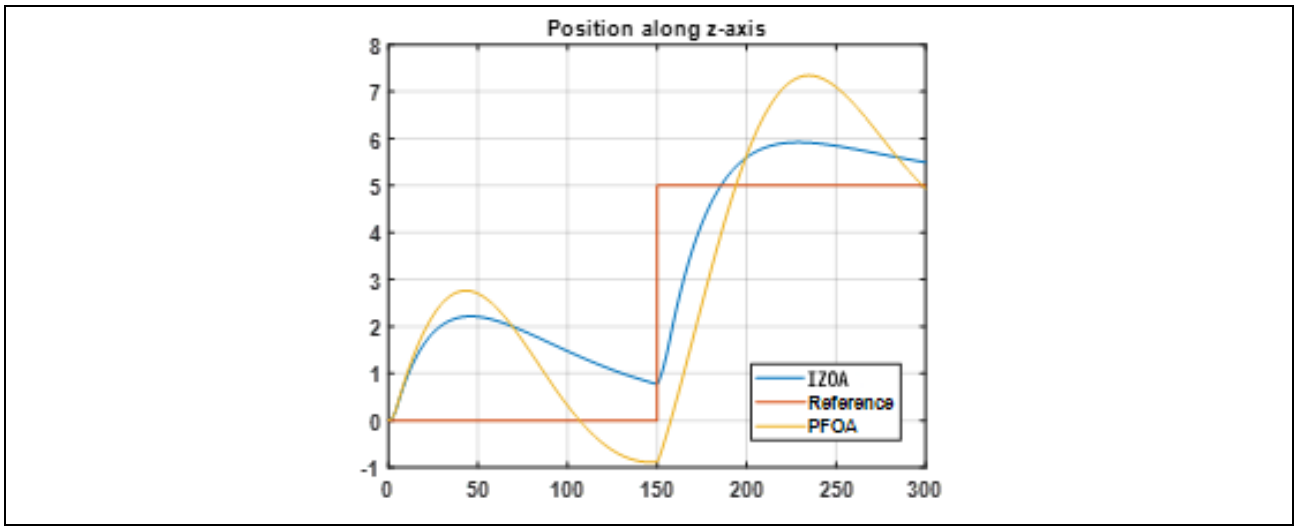

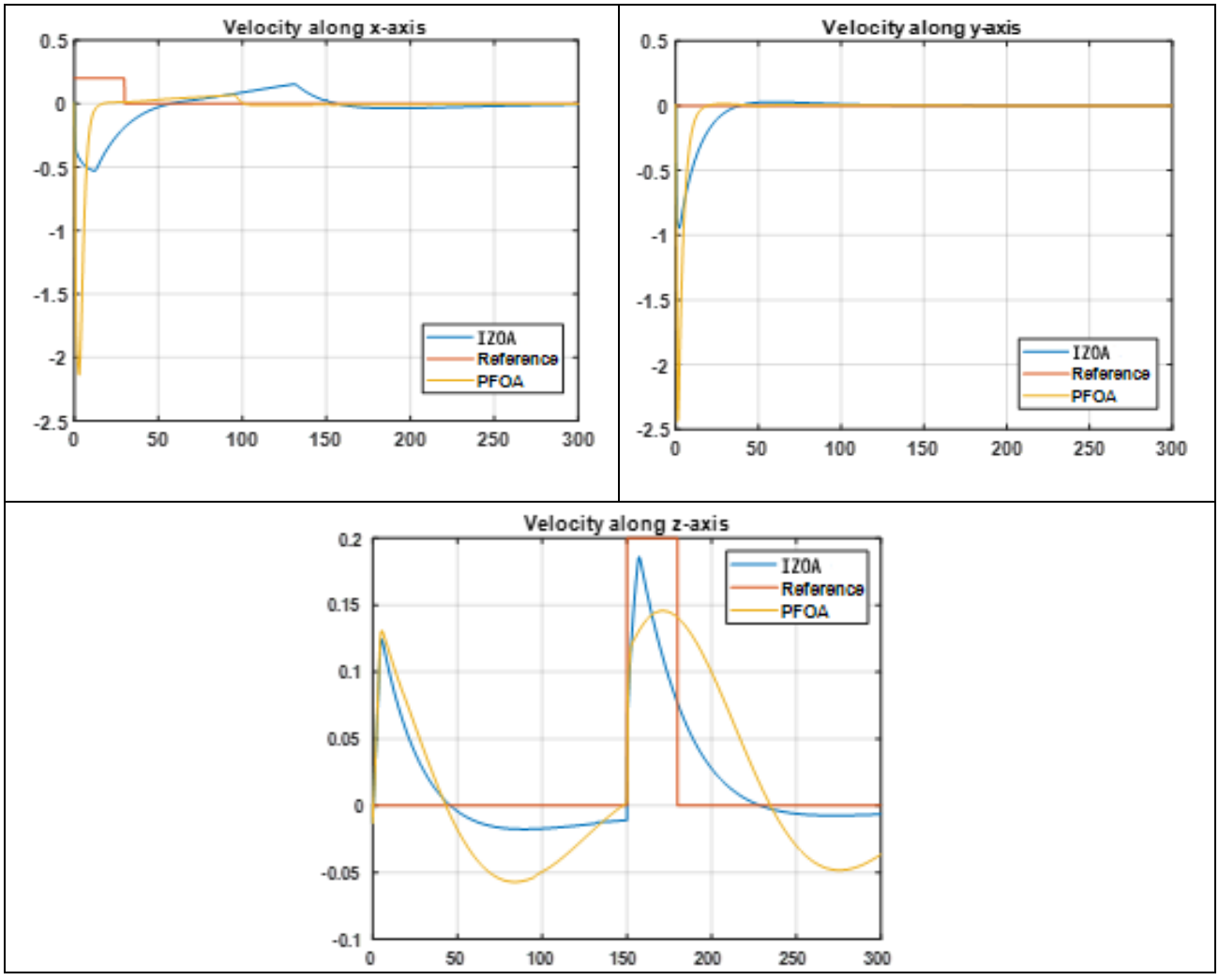

This simulation introduces external noise to test the controller's robustness in maintaining position accuracy. The plot highlights minor fluctuations around the set trajectory due to noise but shows the system's resilience, as the AUV quickly compensates for disturbances and converges to the desired position, ensuring reliability in noisy environments.

7 Conclusion

The study successfully addressed the critical challenges in AUV control by developing a robust control strategy combining a Fractional Order PID controller with the Improved Pufferfish Optimization Algorithm. The integration of IZOA demonstrated significant improvements in convergence rate, computational efficiency, and control precision compared to conventional optimization algorithms. Simulation results validated the effectiveness of the proposed approach in enhancing the performance of AUVs, particularly in trajectory tracking and stability under non-linear dynamics and external disturbances. This research underscores the potential of IZOA in solving complex optimization problems and optimizing control strategies for underwater vehicles. Future work could explore real-time implementation and adaptation to broader operational conditions, further advancing AUV capabilities in marine applications.

8 References

[1] V. Kopman, N. Cavaliere, and M. Porfiri, "MASUV-1: A miniature underwater vehicle with multidirectional thrust vectoring for safe animal interactions," *IEEE/ASME Trans. mechatronics*, vol. 17, no. 3, pp. 563–571, 2011.
[2] T. K. Podder and N. Sarkar, "Fault-tolerant control of an autonomous underwater vehicle under thruster redundancy," *Rob. Auton. Syst.*, vol. 34, no. 1, pp. 39–52, 2001.
[3] K. Tanakitkorn, P. A. Wilson, S. R. Turnock, and A. B. Phillips, "Depth control for an over-actuated, hover-capable autonomous underwater vehicle with experimental verification," *Mechatronics*, vol. 41, pp. 67–81, 2017.
[4] T. Liu, Y. Hu, H. Xu, Q. Wang, and W. Du, "A novel vectored thruster based on 3-RPS parallel manipulator for autonomous underwater vehicles," *Mech. Mach. Theory*, vol. 133, pp. 646–672, 2019.
[5] B. Xin, L. Xiaohui, S. Zhaocun, and Z. Yuquan, "A vectored water jet propulsion method for autonomous underwater vehicles," *Ocean Eng.*, vol. 74, pp. 133–140, 2013.
[6] T. Liu, Y. Hu, H. Xu, Z. Zhang, and H. Li, "Investigation of the vectored thruster AUVs based on 3SPS-S parallel manipulator," *Appl. Ocean Res.*, vol. 85, pp. 151–161, 2019.
[7] R. Panish, "Dynamic control capabilities and developments of the Bluefin robotics AUV fleet," in *Proc. 16th International Symposium on Unmanned Untethered Submersible Technology*, 2009.
[8] D. W. Caress *et al.*, "High-resolution multibeam, sidescan, and subbottom surveys using the MBARI AUV D. Allan B," *Mar. habitat Mapp. Technol. Alaska*, pp. 47–69, 2008.
[9] P. S. Londhe, M. Santhakumar, B. M. Patre, and L. M. Waghmare, "Task space control of an autonomous underwater vehicle manipulator system by robust single-input fuzzy logic control scheme," *IEEE J. Ocean. Eng.*, vol. 42, no. 1, pp. 13–28, 2016.
[10] B. M. Patre, P. S. Londhe, L. M. Waghmare, and S. Mohan, "Disturbance estimator based non-singular fast fuzzy terminal sliding mode control of an autonomous underwater vehicle," *Ocean Eng.*, vol. 159, pp. 372–387, 2018.
[11] P. Herman, "Decoupled PD set-point controller for underwater vehicles," *Ocean Eng.*, vol. 36, no. 6–7, pp. 529–534, 2009.
[12] T. I. Fossen, "Guidance and control of ocean vehicles," *Univ. Trondheim, Norway, Print. by John Wiley Sons, Chichester, England, ISBN 0 471 94113 1, Dr. Thesis*, 1999.
[13] S. Miyamaoto *et al.*, "Maneuvering control system design for autonomous underwater vehicle," in *MTS/IEEE Oceans 2001. An Ocean Odyssey. Conference Proceedings (IEEE Cat. No. 01CH37295)*, IEEE, 2001, pp. 482–489.
[14] P. Sarhadi, A. R. Noei, and A. Khosravi, "Model reference adaptive PID control with anti-windup compensator for an autonomous underwater vehicle," *Rob. Auton. Syst.*, vol. 83, pp. 87–93, 2016.
[15] A. Malerba and G. Indiveri, "Complementary control of the depth of an underwater robot," *IFAC Proc. Vol.*, vol. 47, no. 3, pp. 8971–8976, 2014.
[16] G. Antonelli, S. Chiaverini, N. Sarkar, and M. West, "Adaptive control of an autonomous underwater vehicle: experimental results on ODIN," *IEEE Trans. Control Syst. Technol.*, vol. 9, no. 5, pp. 756–765, 2001.
[17] J.-H. Li and P.-M. Lee, "Design of an adaptive nonlinear controller for depth control of an autonomous underwater vehicle," *Ocean Eng.*, vol. 32, no. 17–18, pp. 2165–2181, 2005.
[18] B. K. Sahu and B. Subudhi, "Adaptive tracking control of an autonomous underwater vehicle," *Int. J. Autom. Comput.*, vol. 11, no. 3, pp. 299–307, 2014.
[19] G. Antonelli, "On the use of adaptive/integral actions for six-degrees-of-freedom control of autonomous underwater vehicles," *IEEE J. Ocean. Eng.*, vol. 32, no. 2, pp. 300–312, 2007.
[20] C. Barbalata, V. De Carolis, M. W. Dunnigan, Y. R. Petillot, and D. M. Lane, "An adaptive controller for autonomous underwater vehicles.," in *IROS*, 2015, pp. 1658–1663.
[21] R. Rout and B. Subudhi, "Inverse optimal self-tuning PID control design for an autonomous underwater vehicle," *Int. J. Syst. Sci.*, vol. 48, no. 2, pp. 367–375, 2017.
[22] H. Wang, Y., Karimi, H. R., Lam, H. K., & Yan, "Fuzzy output tracking control and filtering for nonlinear discrete-time descriptor systems under unreliable communication links.," 2019.
[23] D. Healey, A. J., & Lienard, "Multivariable sliding mode control for autonomous diving and steering of unmanned underwater vehicle.
[24] B. Salgado-Jimenez, T., & Jouvencel, "Using a high order sliding modes for diving control a torpedo autonomous

underwater vehicle. In Oceans 2003. Celebrating the Past... Teaming Toward the Future (IEEE Cat. No. 03CH37492) (Vol. 2, pp. 934-939). IEEE.," 2003.
[25] S. Liang, X., Wan, L., Blake, J. I., "Path following of an underactuated AUV based on fuzzy backstepping sliding mode control. International Journal of Advanced Robotic Systems, 13(3), 122.," 2016.
[26] N. F. Zain, Z. M., & Harun, "Backstepping control strategy for an underactuated x4-auv. Jurnal Teknologi, 74(9).," 2015.
[27] A. L. V. Steenson, A. B. Phillips, E. Rogers, M. E. Furlong and S. R, "Turnock, 'Experimental verification of a depth controller using model predictive control with constraints onboard a thruster actuated auv,' IFAC Proceedings Volumes," no. vol. 45, 5, pp. 275–280, 2012., 2012.
[28] B. Shen, C., Shi, Y., & Buckham, "Model predictive control for an AUV with dynamic path planning. In 2015 54th Annual Conference of the Society of Instrument and Control Engineers of Japan (SICE) (pp. 475-480). IEEE.," 2015.
[29] N. Liu, Y. C., Liu, S. Y., & Wang, "Fully-tuned fuzzy neural network based robust adaptive tracking control of unmanned underwater vehicle with thruster dynamics. Neurocomputing, 196, 1-13.," 2016.
[30] and D. P. V. De Ven, C. Flanagan, "'Neural network control of underwater vehicles,' Engineering Applications of Artificial Intelligence," no. vol. 18, 5, pp. 533–547, 2005., 2005.
[31] K. Shojaei, "'Neural network formation control of under_actuated autonomous underwater vehicles with saturating actuators,' Neurocomputing," vol. 194, 2016.
[32] and Y. L. F. Wang, Y. Xu, L. Wan, "'Real-time control of autonomous underwater vehicles based on fuzzy neural network,' in Proceedings of the 2009 International Workshop on Intelligent Systems and Applications, IEEE, pp. 1–5, Wuhan, China, May 2009," 2009.
[33] et al. Zhang, Jialei, "'Approach-angle-based three-dimensional indirect adaptive fuzzy path following of under-actuated AUV with input saturation.' Applied Ocean Research 107 (2021): 102486.," 2021.
[34] K. Shojaei, "'(ree-dimensional neural network tracking control of a moving target by underactuated autonomous underwater vehicles,' Neural Computing and Applications," vol. 31, n, 2019.
[35] and C. K. A. Z. Zhong, Y. Zhu, "'Reachable set estimation for takagi-sugeno fuzzy systems against unknown output delays with application to tracking control of auvs,' ISA Transactions," vol. 78, p, 2018.
[36] G. Che and Z. Yu, "'Neural-network estimators based fault_tolerant tracking control for auv via adp with rudders faults and ocean current disturbance,' Neurocomputing, vol. 411, pp. 442–454, 2020.," 2020.
[36] O. Elhaki and K. Shojaei, "'A robust neural network ap_proximation-based prescribed performance output-feedback controller for autonomous underwater vehicles with actuators saturation,' Engineering Applications of Artificial Intelligence," vol. 88, p, 2020.
[37] T. I. Fossen, "Handbook of marine craft hydrodynamics and motion control," *John Willy Sons Ltd*, 2011.